

## Article

# An Improved Suppression Method of AC Transient Overvoltage for Line Commuted Converter Based High Voltage Direct Current Considering AC-DC System Coupling

Jinxin Ouyang <sup>1,\*</sup>, Yujie Chen <sup>1</sup>, Xinyu Pan <sup>1</sup> and Yanbo Diao <sup>2</sup>

<sup>1</sup> State Key Laboratory of Power Transmission Equipment Technology, Chongqing University, Chongqing 400044, China; 202211131234@stu.cqu.edu.cn (Y.C.); 202111021053@stu.cqu.edu.cn (X.P.)

<sup>2</sup> Department of Civil Affairs and Social Governance, Chongqing City Management College, Chongqing 401331, China; dyb00820@163.com

\* Correspondence: jinxinoy@cqu.edu.cn

**Abstract:** Commutation failures in line commuted converter-based high voltage direct current (LCC-HVDC) transmission systems leads to an increase in the converter bus voltage of the rectifier station, thus resulting in AC transient overvoltage in the sending-end grid. The transient overvoltage could lead to the disconnection of renewable energy generation and threaten the stable operation of the sending-end grid. However, the influences of the coupling between AC and DC systems caused by the interaction between the active and reactive power of the sending-end grid, the AC bus voltage of the rectifier station, and the DC current are ignored. The AC transient overvoltage cannot be accurately suppressed. Therefore, in this study, the transient voltage characteristics of the rectifier station under a commutation failure of the inverter station are analyzed. The influence of LCC-HVDC control on the AC bus voltage of a rectifier station through the active and reactive power of the rectifier station is analyzed. A dynamic model of the AC bus voltage of a rectifier station under an AC-DC system coupling is established. The calculation method of the command value of the DC current of the rectifier station is proposed by a predictive control model, and an improved suppression method for AC transient overvoltage is proposed. The case studies show that the accuracy and effectiveness of the suppression of AC transient overvoltage are improved by considering the coupling between AC and DC systems.

**Keywords:** line commuted converter based high voltage direct current transmission system (LCC-HVDC); transient overvoltage; AC-DC system coupling; DC current control



**Citation:** Ouyang, J.; Chen, Y.; Pan, X.; Diao, Y. An Improved Suppression Method of AC Transient Overvoltage for Line Commuted Converter Based High Voltage Direct Current Considering AC-DC System Coupling. *Electronics* **2024**, *13*, 1844. <https://doi.org/10.3390/electronics13101844>

Academic Editor: Raffaele Giordano

Received: 21 April 2024

Revised: 6 May 2024

Accepted: 7 May 2024

Published: 9 May 2024



**Copyright:** © 2024 by the authors. Licensee MDPI, Basel, Switzerland. This article is an open access article distributed under the terms and conditions of the Creative Commons Attribution (CC BY) license (<https://creativecommons.org/licenses/by/4.0/>).

## 1. Introduction

Line commuted converter-based high voltage direct current (LCC-HVDC) transmission systems have the advantages of long transmission distance and large transmission capacity. Thus, LCC-HVDC is widely used to transmit renewable energy [1–3]. Thyristors without self-turn-off capability are used as converter devices in LCC-HVDC. Inverter stations are prone to commutation failures following faults in the receiving-end grid. Commutation failures cause the AC bus voltage of the rectifier station to decrease first, and then increase, which produces AC transient overvoltage in the sending-end grid. The AC transient overvoltage may cause the renewable energy generation to be disconnected from the grid, and even threaten the stable operation of the sending-end grid. Both the sending-end grid and LCC-HVDC are faced with a serious threat due to AC transient overvoltage.

The suppression of AC transient overvoltage has gained a lot of attention. The authors of [4] pointed out that DC current overshooting in the rectifier station leads to reactive power surplus and AC transient overvoltage in the sending-end grid when commutation failure occurs in the inverter station. The transient reactive power characteristics of the

sending-end and receiving-end grid during commutation failures and their effects on the AC transient overvoltage are analyzed [5]. The authors of [6] provided an expression for the peak value of AC transient overvoltage. The influencing factors of feeder AC transient overvoltage have been quantitatively analyzed [7]. The existing studies have focused on the effect of the change in reactive power consumption of the rectifier station due to the change in active power caused by the commutation failure. The direct effect of active power on the AC bus voltage has thus far been neglected in the literature.

There are two main types of methods used for the suppression of AC transient overvoltage. Reactive power compensation is the more effective way. Reactive power compensation can reduce the reactive power compensated by the filter, and mitigate reactive power surplus during low-voltage periods. Additionally, during overvoltage conditions, reactive power compensation devices absorb a portion of the reactive power, providing a significant amount of capacitive reactive power to the grid. Reactive power compensation devices help to mitigate excess reactive power at the rectifier station, thereby suppressing the AC transient overvoltage. Commonly used reactive power compensation devices include the static var compensator (SVC), static synchronous compensator (STATCOM), and phase angle regulators. The regulator capacity is selected according to the size of the transient overvoltage [8]. Transient overvoltage suppression strategies that coordinate the converter station filter, synchronous compensator, and synchronous generator in the near zone of the converter station have been proposed [9,10]. Additionally, an optimization control model has been constructed to reduce the AC transient overvoltage by coordinating a synchronous compensator and a static var compensator [11,12]. Dynamic reactive power compensation can suppress the AC transient overvoltage, but the investment cost is high and the coordination between reactive power compensation devices is complicated. The utilization of reactive power compensation to prevent AC transient overvoltage is limited. However, the substantial reactive power consumption of LCC-HVDC incurs high costs when installing dynamic reactive power compensation devices, and it also escalates the coordination complexity between the converter station and dynamic reactive power compensation devices. Therefore, current research often involves optimizing the control system of LCC-HVDC to suppress transient overvoltage at the rectifier station.

Suppressing the AC transient overvoltage by optimizing the control system of LCC-HVDC is a hot spot in current research. A parameter optimization method to suppress the AC transient overvoltage according to the sensitivity relationship between control parameters and the AC transient overvoltage has been proposed [13]. The parameters of the voltage-dependent current order limiter (VDCOL), commutation failure prevention control, and constant current control (CCC) have been optimized to reduce the reactive power exchanged between the rectifier station and the grid during the fault period [5,14]. In one study, the reference value of the trigger angle of the rectifier station was improved to suppress the transient overvoltage according to the relationship between the reactive power consumed by the rectifier station, the DC voltage, and the DC current [15,16]. The trigger angle can also be determined according to the load flow of the sending-end grid and the relationship between the reactive power and voltage [17].

The sending-end grid and rectifier station are connected by the power flow. The variation in the AC bus voltage of the rectifier station changes the active and reactive power of the rectifier station, which further affects the AC bus voltage. The AC-DC system coupling is aggravated in the sending-end grid with a small short-circuit ratio, because the change in the active power has a greater effect on the AC bus voltage of the rectifier station. Coupling AC and DC systems influence each other through line connections. The authors of [18] analyzed the mutual influence among control parameters of AC and DC systems under normal operation, while the authors of [19] examined the interaction characteristics of AC and DC systems from the perspectives of large and small disturbances, providing a comprehensive overview of the causes, phenomena, and consequences of various interactions. The authors of [20] analyzed the coupling characteristics between LCC-HVDC and the weak sending-end grid, indicating that large-scale power transfer

resulting from LCC-HVDC faults can lead to voltage instability or even transient instability in power grids. The authors of [21] established quantitative evaluation indices for the coupling between AC and DC systems in multi-infeed DC transmission systems based on electrical quantities, such as the inter-tie impedance between converter stations, DC power, and short-circuit capacity. The authors of [22] analyzed the influencing factors of transient overvoltage, clarifying the transient voltage characteristics and dominant influencing factors under AC and DC system faults and categorizing the influencing factors of transient overvoltage in the sending-end grid into three types: LCC-HVDC control parameters, the sending-end grid, and the receiving-end grid faults. The authors of [23] pointed out that during the generation of transient overvoltage in the sending-end grid, changes occur in variables such as the rectifier station AC bus voltage, the reactive power consumption of the rectifier station, and the DC current. These changes trigger rapid responses from relevant controllers in LCC-HVDC to maintain grid stability. Conversely, the controlled electrical quantities then influence the control process, forming a cyclic relationship. The AC transient overvoltage is suppressed by adjusting the reactive power consumed by the rectifier station in the existing method. Because the active and reactive power of LCC-HVDC is coupled, the adjustment of reactive power inevitably changes the active power. The variation in active power leads to a change in AC bus voltage, which affects the active and reactive powers. Neglecting the AC-DC system coupling at the rectifier station could affect the accuracy of transient overvoltage suppression.

In this study, the AC transient voltage characteristics of the sending-end grid of LCC-HVDC under commutation failure are analyzed with consideration for the joint influence of active and reactive power changes. Additionally, the impact of AC-DC system coupling on the AC transient overvoltage is explored. The expression of the AC bus voltage of the rectifier station is derived to depict the relationship between the AC bus voltage and DC current under the action of AC-DC system coupling. A dynamic model of the AC bus voltage is established considering AC-DC system coupling. Then, an improved suppression method for AC transient overvoltage considering the AC-DC system coupling is proposed, which is realized by setting the command value of the DC current of the rectifier station based on model prediction control. The effectiveness of the proposed method is verified by the standard test model of the LCC-HVDC.

## 2. Transient Voltage Characteristics of Sending-End Grid

The structure of LCC-HVDC, which mainly includes converter stations and a DC transmission line, is shown in Figure 1. The converter station includes a rectifier station and an inverter station. The rectifier and inverter stations are connected through DC transmission lines. Filters are equipped in the DC and AC sides of converter stations. A hierarchical control structure is adopted in LCC-HVDC. The main control level sends the commands from the dispatching center to the pole control level after calculating and processing. The pole control level sends the control signal to the control units of the converter valves. Then, the normal phase change is realized through controlling the conductance of the converter valves. The minimum trigger angle control and CCC are deployed in the rectifier station. The constant current control, current error control (CEC), and constant extinction angle control (CEAC) are deployed in the inverter station. Both rectifier and inverter stations are configured with VDCOL [24]. During the steady-state operation of LCC-HVDC, the rectifier station is generally controlled by CCC, and the inverter station is controlled by CEAC [25]. During commutation failures of the inverter station, the rectifier station typically utilizes CCC and VDCOL to maintain the DC current.

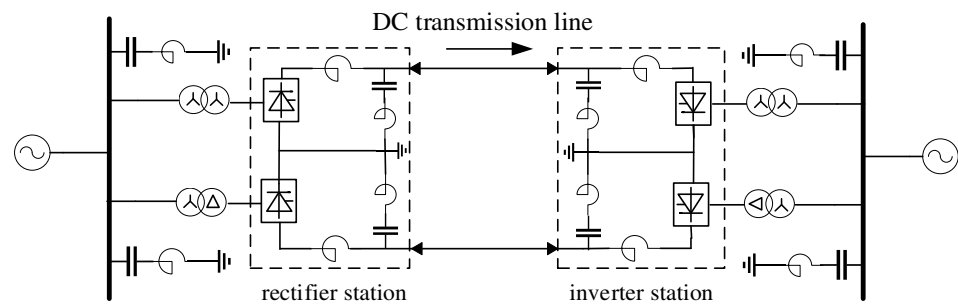


Figure 1. High voltage direct current transmission system.

A commutation failure occurs when a valve expected to turn off fails to regain the blocking ability under reverse voltage or cannot complete the turn-off process, which causes an inverse commutating phase from the valve expected to turn off to the valve expected to turn on. The DC current changes under the combined action of the control of the inverter and rectifier stations, which results in fluctuations in active power and reactive power consumption at the rectifier station. The power fluctuations change the AC bus voltage of the rectifier station, as shown in Figure 2. The transient of LCC-HVDC after commutation failure can be divided into four stages.

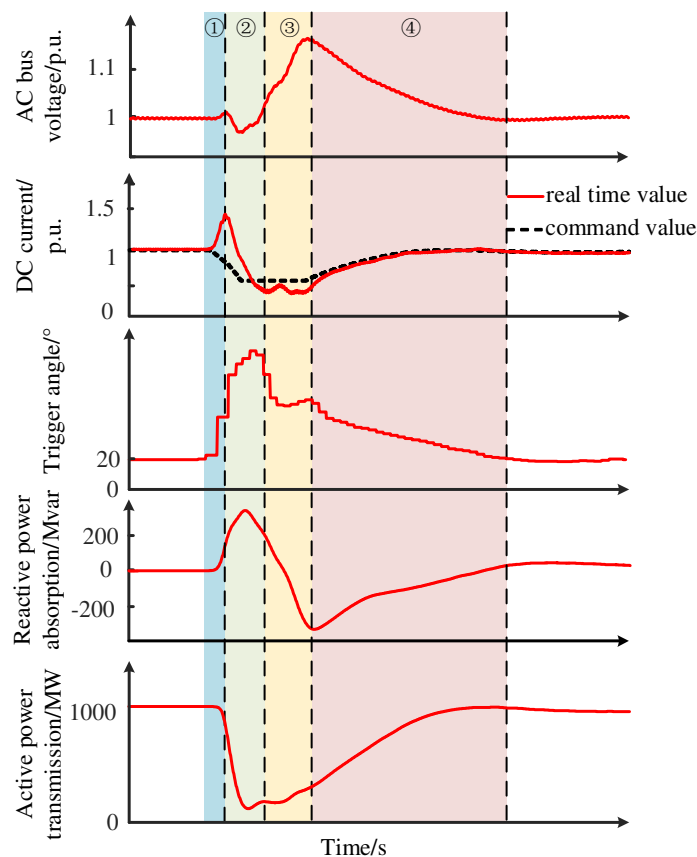


Figure 2. Transient processes of LCC-HVDC.

Stage 1: Both valves of the upper and lower bridge arms conduct simultaneously after a commutation failure. The commutation failure leads to a short circuit on the DC side. The DC voltage at the inverter station reduces, thus resulting in a rapid surge in DC current. The sudden surge in DC current causes a slight uptick in the AC bus voltage of the rectifier station because of the delayed response of the rectifier station controllers.

Stage 2: The command value of the DC current decreases as the DC voltage decreases under the action of VDCOL. While the CCC of the rectifier station controls the trigger angle to increase briefly to reduce the DC current, the DC current gradually approaches the command value. However, because the DC current is still larger than the steady-state value and the trigger angle of the rectifier station increases, the reactive power consumed by the rectifier station increases. The rectifier station absorbs more reactive power from the sending-end grid. At the same time, the active power transmission is blocked due to the drop in DC voltage at the inverter station [26]. Therefore, the AC bus voltage drops.

Stage 3: Normal commutation is recovered. The DC voltage of the inverter station gradually increases. The trigger angle of the rectifier station reduces, but also maintains a considerable value. Concurrently, the DC current of the rectifier station continues to decrease to the commanded value of the VDCOL. As the DC current stabilizes, the transmission power remains relatively constant. However, the decrease in the DC current prompts a notable reduction in the consumed reactive power. Because of the constraints of the response speed of the AC filter and the communication delay, the reactive power compensation at the rectifier station cannot be decreased in a timely manner. The surplus reactive power is delivered to the sending-side grid, thus resulting in a rise in the AC bus voltage of the rectifier station.

Stage 4: The DC voltage at the inverter station gradually rises and returns to the rated value under the influence of the control system after the fault clearance. Simultaneously, the DC current gradually returns to the normal value. The trigger angle of the rectifier station decreases gradually, restoring the active power to the pre-fault level. The reactive power consumed by the rectifier station gradually resumes. The sending-end grid supplies more active power to the rectifier station, leading to a balance in the exchange of reactive power between the rectifier station and the sending-end grid. Consequently, the AC bus voltage of the rectifier station gradually returns to the steady-state value.

After a commutation failure of the inverter station, the active power of the rectifier station decreases initially, then gradually increases due to the intervention of the control system. The reactive power consumed by the rectifier station initially rises before subsequently decreasing. Under the influence of active and reactive power, the AC bus voltage of the rectifier station decreases initially before rising. The increase in AC bus voltage leads to transient overvoltage in the sending-end grid, posing a threat to renewable energy generation.

### 3. AC-DC System Coupling and Its Effects

#### 3.1. Mathematical Analysis of AC Bus Voltage

Figure 3 shows the sending-end grid of LCC-HVDC.  $U_{Lr}$  is the AC bus voltage of the rectifier station;  $U_{oc}$  is the voltage of the sending-end grid;  $R_r$  and  $X_r$  are the equivalent resistance and the reactance of the sending-end grid, respectively; and  $P_{oc}$  and  $Q_{oc}$  are the active and reactive power provided by the sending-end grid, respectively. The active and reactive power of the rectifier station satisfy:

$$\begin{cases} P_{ac} = U_{dr} I_{dr} \\ Q_{dr} = Q_{ac} + Q_{cr} \end{cases} \quad (1)$$

where  $P_{ac}$  and  $Q_{ac}$  are the active and reactive power fed to the rectifier station from the sending-end grid, respectively;  $Q_{dr}$  is the reactive power consumed by the rectifier station; and  $Q_{cr}$  is the reactive power compensated by the filter.

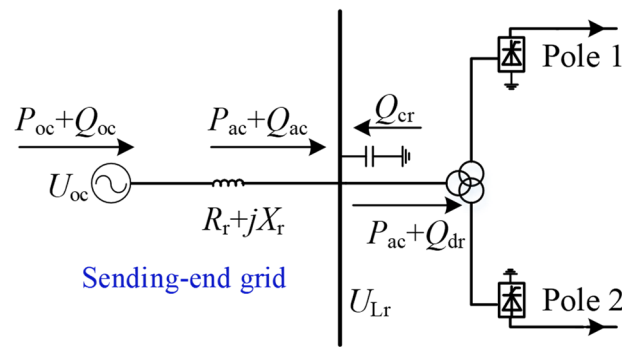


Figure 3. Sending-end grid of LCC-HVDC.

The reactive power consumed by the rectifier station is related to the active power, and can be written as [27]:

$$Q_{dr} = P_{ac} \tan \varphi_r = P_{ac} \frac{\mu_r - \sin \mu \cos(2\alpha_r + \mu_r)}{\sin \mu \cos(2\alpha_r + \mu_r)} \quad (2)$$

where  $\varphi_r$  is the power factor angle of the rectifier station;  $\mu_r$  is the phase change overlap angle of the rectifier station; and  $\alpha_r$  is the trigger angle of rectifier station.

Based on the power flow relationship between the rectifier station and the sending-end grid, the voltage phasor of the sending-end grid can be expressed as:

$$U_{oc} \angle \theta_1 = U_{Lr} \angle \theta_2 + \frac{P_{ac} - jQ_{ac}}{U_{Lr} \angle -\theta_2} (R_r + jX_r) \quad (3)$$

where  $\theta_1$  and  $\theta_2$  are the phase angles of the sending-end grid and the AC bus of the rectifier station, respectively.

Substituting Equation (1) into Equation (3) and simplifying, Equation (3) can be written as:

$$U_{oc} U_{Lr} \cos(\theta_2 - \theta_1) - j U_{oc} U_{Lr} \sin(\theta_2 - \theta_1) = U_{Lr}^2 + (P_{ac} R_r + Q_{ac} X_r) + j(P_{ac} X_r - Q_{ac} R_r) \quad (4)$$

The voltage phase of the sending-end grid is set as the reference. Because the real and imaginary parts of both sides of the equation are respectively equal, Equation (4) can be written as:

$$\begin{cases} U_{oc} U_{Lr} \cos \theta_2 = U_{Lr}^2 + (P_{ac} R_r + Q_{ac} X_r) \\ U_{oc} U_{Lr} \sin \theta_2 = -(P_{ac} X_r - Q_{ac} R_r) \end{cases} \quad (5)$$

Because  $\cos^2 \theta_2 + \sin^2 \theta_2 = 1$ , Equation (5) can be organized as:

$$U_{Lr}^4 + U_{Lr}^2 [2(P_{ac} R_r + Q_{ac} X_r) - U_{oc}^2] + (P_{ac} X_r - Q_{ac} R_r)^2 = 0 \quad (6)$$

LCC-HVDC is mainly used in high-voltage grids. The resistance is much smaller than the reactance. Therefore, the resistance is neglected. Solving Equation (6), the AC bus voltage of a rectifier station under the combined influence of active and reactive power can be obtained as:

$$\frac{[U_{Lr}^2 - (U_{oc}^2/2 - Q_{ac} X_r)]^2}{(U_{oc}^4 - 4Q_{ac} X_r U_{oc}^2)/2} + \frac{X_r^2}{(U_{oc}^4 - 4Q_{ac} X_r U_{oc}^2)/2} P_{ac}^2 = 1 \quad (7)$$

After a commutation failure, variations in the electrical quantities at the rectifier station lead to corresponding changes in the sending-end grid. Under a constant transmitted reactive power, the relationship between the active power fed to the rectifier station and the AC bus voltage is shown in Figure 4a. With positive active power, the square of the AC bus voltage is inversely proportional to the active power. The smaller the AC bus voltage,

the more active power is supplied to the rectifier station by the sending-end grid. Under constant transmitted active power, the relationship between the AC bus voltage of the rectifier station and the reactive power fed to the rectifier station is shown in Figure 4b. The square of the AC bus voltage is inversely proportional to the reactive power fed to the rectifier station. The lower the reactive power, the higher the AC bus voltage of the rectifier station.

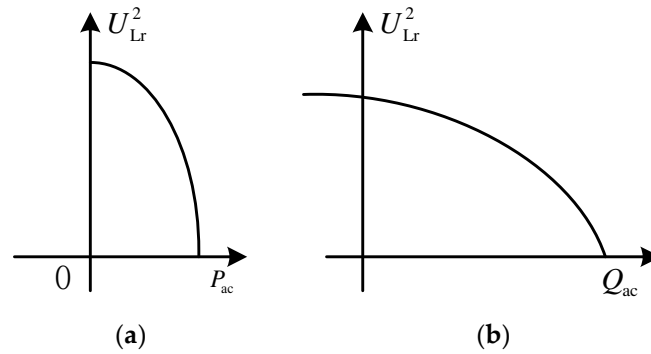


**Figure 4.** Relationship between the AC bus voltage and power. (a) Active power and voltage; (b) reactive power and voltage.

When the active and reactive power changes, the AC bus voltage can be expressed as [15]:

$$U_{Lr} = \sqrt{(U_{LrN} + \Delta U_{Lr})^2 + (\delta U_{Lr})^2} \tag{8}$$

where  $U_{LrN}$  is the AC bus voltage under normal operation;  $\Delta U_{Lr}$  and  $\delta U_{Lr}$  are, respectively, the transverse component of voltage variation caused by reactive power, and the longitudinal component of voltage variation caused by active power, which can be given by:

$$\begin{cases} \Delta U_{Lr} = \frac{\Delta Q_r U_{LrN}}{SCR \times P_{dN}} \\ \delta U_{Lr} = \frac{\Delta P_r U_{LrN}}{SCR \times P_{dN}} \end{cases} \tag{9}$$

where  $\Delta Q_r$  and  $\Delta P_r$  are the reactive power imbalance and the active power variation in the rectifier station, respectively; SCR is the short-circuit ratio of the sending-end grid; and  $P_{dN}$  is the rated transmission power of LCC-HVDC.

The impact of variations in active and reactive power on the AC bus voltage is dependent on the short-circuit ratio of the sending-end grid. When the short-circuit ratio is high, the effect of variations in active power on the AC bus voltage is limited. However, when the short-circuit ratio is low, the impact of variations in active power becomes more pronounced. The transient voltage is influenced by both active and reactive power variations.

### 3.2. Effect of AC-DC System Coupling on Transient Overvoltage

Under the power flow constraints of the sending-end grid, the AC transient overvoltage in the sending-end grid is related to both active and reactive power. The DC voltage can be expressed as:

$$U_{dr} = \frac{3}{\pi} \sqrt{2} N k_r U_{Lr} \cos \alpha_r - \frac{3}{\pi} N X_s I_{dr} \tag{10}$$

where  $N$  is the number of six pulsating converters in each pole of the rectifier station;  $k_r$  is the ratio of the converter transformer of the rectifier station; and  $X_s$  is the commutation reactance of the rectifier station.

According to Equations (1) and (10), the active power fed to the rectifier station can be obtained as:

$$P_{ac} = \frac{3}{\pi} \sqrt{2} N k_r U_{Lr} \cos \alpha_r I_{dr} - \frac{3}{\pi} N X_s I_{dr}^2 \tag{11}$$

The reactive power consumed by the rectifier station can be expressed as:

$$Q_{dr} = I_{dr} \sqrt{U_{dr0}^2 - U_{dr}^2} = I_{dr} \sqrt{-U_{dr}^2 + \frac{18k_r^2 N^2 U_{Lr}^2}{\pi^2}} \quad (12)$$

where  $U_{dr0}$  is the DC no-load voltage of the rectifier station, which can be expressed as:

$$U_{dr0} = 3\sqrt{2}Nk_r U_{Lr} / \pi \quad (13)$$

According to Equation (1), the reactive power fed to the rectifier station from the sending-end grid can be obtained as:

$$Q_{ac} = I_{dr} \sqrt{-U_{dr}^2 + \frac{18k_r^2 N^2 U_{Lr}^2}{\pi^2}} - B_{cr} U_{Lr}^2 \quad (14)$$

The active power fed to the rectifier station is dependent on the trigger angle of the rectifier station and the DC current, while the reactive power fed to the rectifier station is determined by the DC current. The control system of the rectifier station regulates the DC current by adjusting the trigger angle. Adjusting the DC current can change both the active power and reactive power. However, variations in active and reactive power cause variations in the AC bus voltage of the rectifier station. Because the active and reactive power is not decoupled, the variations in AC bus voltage further change the active and reactive power. The power, AC bus voltage, and DC current of the rectifier station interact with each other, resulting in the AC-DC system coupling. The AC transient overvoltage is not only determined by the DC current, but is also related to the power flow of the sending-end grid under the AC-DC system coupling.

#### 4. Transient Overvoltage Suppression Method Considering AC-DC System Coupling

After a commutation failure, the rectifier station absorbs a large amount of reactive power due to the rapid rise in DC current. As the DC current falls, the reactive power consumed by rectifier station decreases, which produces a reactive power surplus. Meanwhile, the obstruction of power transmission results in a decline in the active power fed to the rectifier station. The reactive power imbalance and active power variations jointly result in AC transient overvoltage. Therefore, by substituting Equations (11) and (14) into Equation (7), the dynamic model of the AC bus voltage can be built as:

$$\pi^2 U_{Lr}^2 (-1 + B_{cr} X_r)^2 + 18 I_{dr}^2 k_r^2 N^2 X_r^2 - \pi^2 U_{oc}^2 - 6 I_{dr} \pi X_r (-1 + B_{cr} X_r) \cdot \sqrt{2 N^2 k_r^2 U_{Lr}^2 - N^2 (I_{dr} X_s - \sqrt{2} k_r U_{Lr} \cos \alpha_r)^2} = 0 \quad (15)$$

The trigger angle of the rectifier station varies according to the command value under CCC. The trigger angle can be written as:

$$\alpha_r = \pi - K_{p-ccc} \left\{ [I_{drord} - I_{dr}] + \frac{1}{T_{i-ccc}} \int [I_{drord} - I_{dr}] dt \right\} \quad (16)$$

The trigger angle is related to the DC current, so the dynamic model of the AC bus voltage reflects the relationship between the AC bus voltage and the DC current, which depicts the feasible range of the AC bus voltage of the rectifier station under the coupling effect of the sending-end grid and the rectifier station. The feasible range is related to the DC current. The AC transient overvoltage can be suppressed by controlling the DC current. According to the dynamic model, the improved suppression method of AC transient overvoltage is proposed based on the model of predictive control, as shown in Figure 5.

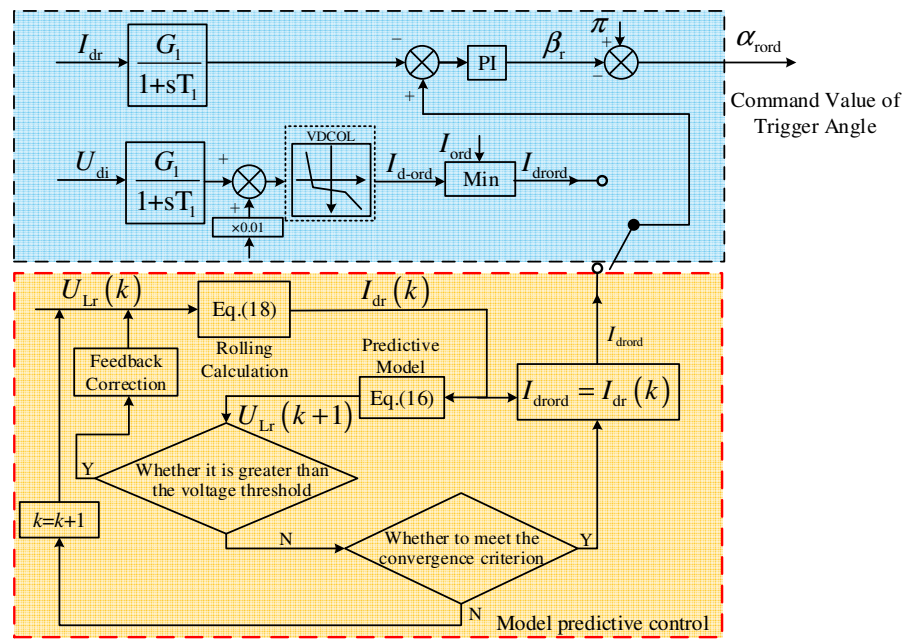


Figure 5. Improved suppression method of AC transient overvoltage.

The model of predictive control takes the output of the previous moment as the input of the next moment until the convergence condition is satisfied, and finally obtains the optimal control command value. The DC current of the rectifier station is used as the control quantity. The command value of the DC current, to prevent the AC bus voltage from exceeding the limit, is determined through continuous iteration. The smaller the AC bus voltage, the larger the DC current variation. A large DC current is not conducive to DC voltage stabilization, nor the commutation recovery of the inverter station. Therefore, controlling the AC bus voltage within the allowable voltage threshold is taken as the control target. The DC current first rises and then decreases after a commutation failure. As the DC current decreases, the AC bus voltage rises. Therefore, VDCOL is switched to overvoltage suppression control when a decrease in the DC current is detected.

Step 1: According to the relationship between AC bus voltage and DC current, the DC current at moment  $k$  is calculated by the AC bus voltage at moment  $k$ , which can be written as:

$$I_{dr}(k) = \frac{U_{Lr}(k)k_r[\cos(\alpha_r(k) + \mu_r(k)) - \cos \alpha_r(k)]}{\sqrt{2}X_s I_{dr}(k)} \tag{17}$$

where  $U_{Lr}(k)$  and  $I_{dr}(k)$  are the AC bus voltage and DC current at moment  $k$ ;  $\alpha_r(k)$  and  $\mu_r(k)$  are the firing angle and overlap angle of commutation at moment  $k$ .

Step 2: Equation (15) is used as a prediction model, and the predicted AC bus voltage at the moment  $k + 1$  can be obtained according to the DC current at the moment  $k$ :

$$U_{Lr}(k+1) = g[I_{dr}(k)] \tag{18}$$

Step 3: The predicted AC bus voltage is compared with the allowable voltage threshold. If the predicted AC bus voltage is greater than the allowable voltage threshold, the feedback correction should be implemented. The AC bus voltage after feedback correction is written as:

$$U_{Lr}'(k) = U_{Lr}(k) - \Delta U \tag{19}$$

where  $\Delta U = U_{Lr}(k+1) - U_{Lr,max}$ , which is the deviation between the voltage at the moment  $k + 1$  and the allowable voltage threshold.

The AC bus voltage at moment  $k$  is replaced by  $U_{Lr}'(k)$ . Then, step 1 is repeated. If the predicted AC bus voltage is less than or equal to the allowable voltage threshold, continue to step 4.

Step 4: The AC voltage difference between the  $k$  and  $k + 1$  moments is judged according to the following convergence criterion:

$$|U_{Lr}(k+1) - U_{Lr}(k)| < \varepsilon \quad (20)$$

where  $\varepsilon$  is a sufficiently small constant.

If the convergence criterion is not satisfied, the AC bus voltage at moment  $k$  is replaced by that at the moment of  $k + 1$ . Then, step 1 is repeated. The iteration repeats until the convergence criterion is satisfied. The DC current that makes the AC bus voltage satisfy the convergence criterion is adopted as the command value. The command value of the trigger angle is generated by the CCC for trigger control. The command value of the DC current takes into account the influence of the AC-DC system coupling on the transient overvoltage, thereby enhancing the accuracy of the control of AC transient overvoltage.

The transient AC overvoltage suppression method proposed in this paper achieves control by dynamically computing the DC current command value in real-time and utilizing the existing CCC to determine the rectifier station's trigger angle command value. This approach requires no additional hardware, only the inclusion of a calculation module for the DC current command value, making it practical in a real system.

## 5. Case Study

Theoretical analyses were verified using PSCAD simulations based on the CIGRE HVDC standard test system. The system parameters were as follows: the rated voltage of the monopole LCC-HVDC was 500 kV, with a base capacity of 1000 MW. Twelve-pulse converters were equipped. The converter transformer reactance was 13.5  $\Omega$ . The short-circuit ratios of the sending- and receiving-end grids were 2.5 $\angle$ 84° and 2.5 $\angle$ 75°, respectively [28]. Under normal operation, the DC current was 2 kA, the commutation angle of the inverter station was 15.2°, and the advanced trigger angle was 38.3°. The voltage threshold of the rectifier station was 1.1 p.u. Different control methods were compared. Method 1: The VDCOL and CCC were adopted in the rectifier station, where the proportional coefficient and integral time constant of CCC were 1.0989 and 0.01092 s, respectively. The upper and lower limits of the DC current for VDCOL were 1.0 p.u. and 0.55 p.u., respectively, with the corresponding thresholds for the DC voltage set at 0.9 p.u. and 0.4 p.u. Method 2: The proposed method. Method 3: A method solely relying on compensating for the reactive power consumption of the rectifier station to suppress AC transient overvoltage [16].

### 5.1. Under Different Fault Types

The short-circuit ratio of the sending-end grid was 2.5. A three-phase fault and a single-phase fault occurred at the AC bus of the inverter station at 1 s, respectively. The transition inductance of the fault was 0.7 H, and the fault duration was 0.1 s. The electrical quantities of LCC-HVDC are shown in Figures 6 and 7. The blue curve indicates Method 1, the red curve indicates Method 2, and the black curve indicates Method 3.

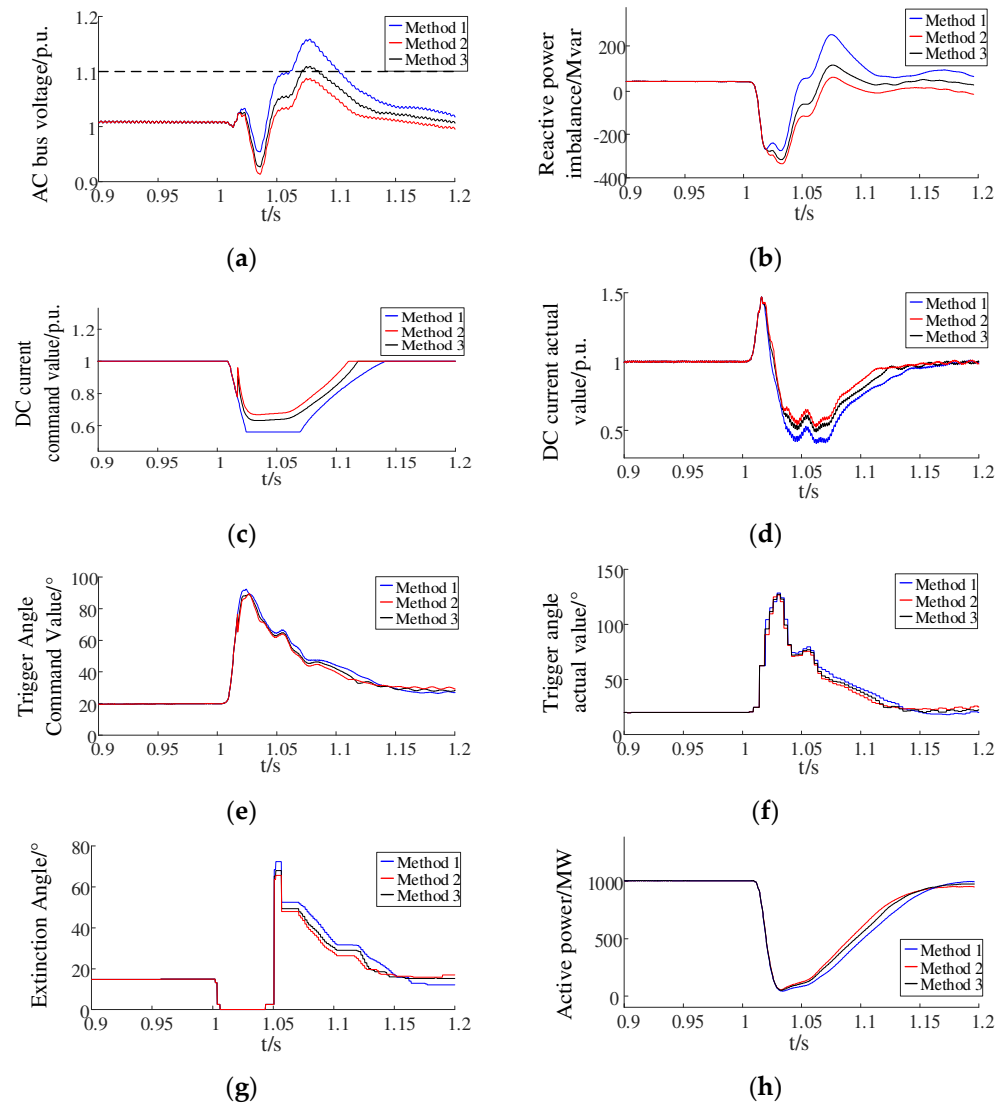


**Figure 6.** Electrical quantities of LCC-HVDC under a three-phase fault (SCR = 2.5). (a) AC bus voltage of rectifier station; (b) Reactive power imbalance; (c) Command value of the DC current at the rectifier station; (d) DC current actual value at the rectifier station; (e) Trigger angle command value of the rectifier station; (f) Trigger angle actual value of the rectifier station; (g) Extinction angle of the inverter station; (h) Active power fed to the rectifier station.

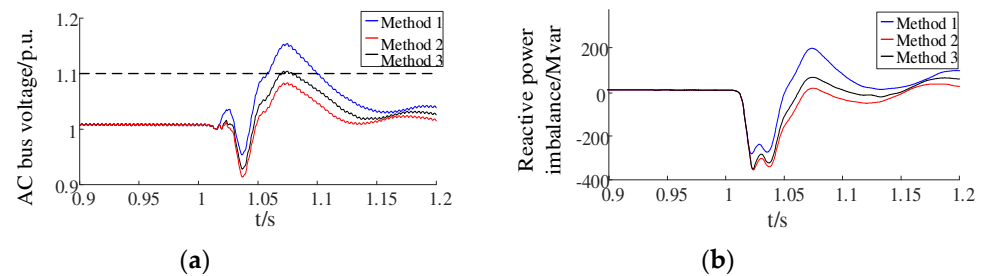


**Figure 7.** Cont.

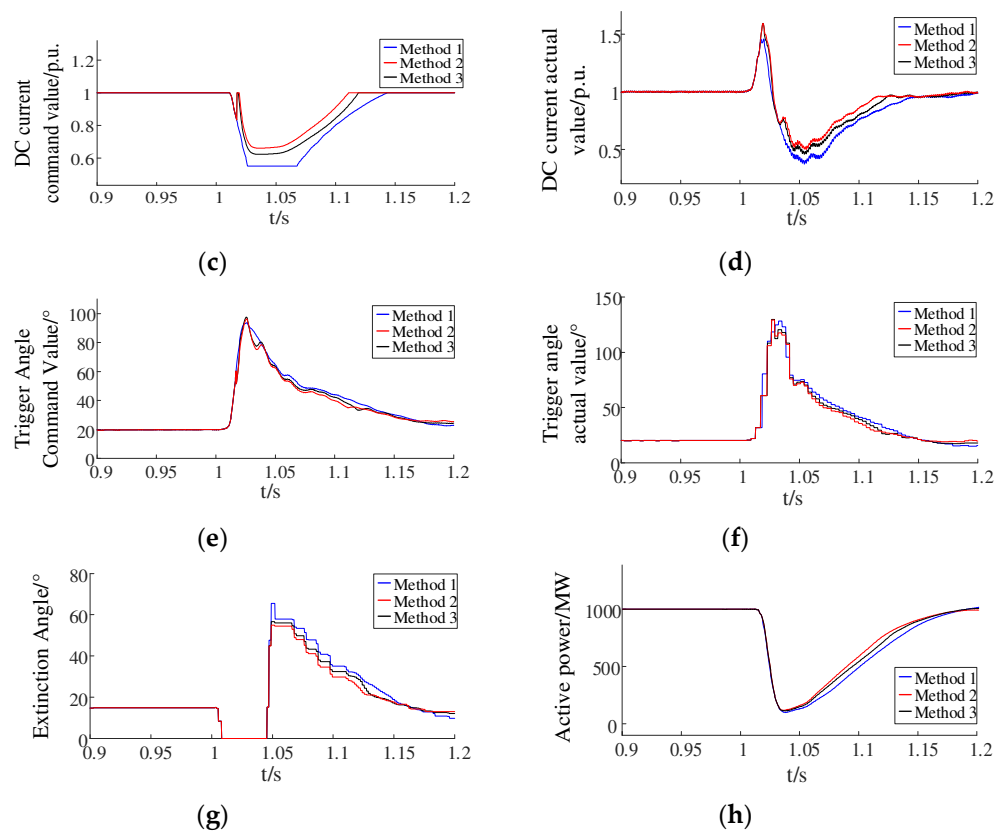


**Figure 7.** Electrical quantities of LCC-HVDC under single-phase fault ( $SCR = 2.5$ ). (a) AC bus voltage of rectifier station; (b) Reactive power imbalance; (c) Command value of the DC current at the rectifier station; (d) DC current actual value at the rectifier station; (e) Trigger angle command value of the rectifier station; (f) Trigger angle actual value of the rectifier station; (g) Extinction angle of the inverter station; (h) Active power fed to the rectifier station.

When a three-phase fault occurred, as shown in Figure 6a, the maximum value of the AC bus voltage under Method 1 was 1.159 p.u., which was more than the allowable voltage threshold. The AC bus voltage was decreased by compensating for the reactive power consumption under Method 3. However, the maximum voltage was 1.109 p.u., which still exceeded the allowable voltage threshold due to neglecting the effects of active power and AC-DC system coupling. The maximum AC bus voltage under Method 2 was 1.087 p.u., which was less than the allowable voltage threshold of 1.1 p.u. The AC transient overvoltage was avoided.

As shown in Figure 6b–d, the command value of the DC current was changed because the control was switched when the DC current was reduced under Method 2. The DC current under Method 2 was greater than that under Method 1 and Method 3 after 1.04 s. The decrease in DC current reduced the reactive power imbalance and thereby reduced the AC bus voltage. As shown in Figure 6e,f, the trigger angle command value under Method 2 was reduced compared to Method 1 and Method 3, and the actual value of the trigger angle was also relatively reduced. As shown in Figure 6h, the active power fed to the rectifier station under Method 2 was increased compared to Method 1 and Method 3. The reduced active power variation and reactive power imbalance caused the AC transient overvoltage to decrease. As shown in Figure 6g, there was no subsequent commutation failure under the three methods. The AC transient overvoltage was prevented by Method 2, without increasing the risk of commutation failure.

As shown in Figure 7a, the maximum AC bus voltage under Method 2 was 1.083 p.u. under a single-phase fault, which accurately prevented overvoltage. The maximum AC bus voltages under Method 1 and Method 3 were 1.154 p.u. and 1.105 p.u., respectively. The AC

bus voltage reduced, but still exceeded the allowable voltage threshold, under Method 3. As shown in Figure 7b–d, the command value of the DC current under Method 2 was greater, so the DC current increased compared to that of Method 1 and Method 3. Under the effects of the DC current, the reactive power imbalance under Method 2 was smaller than that of Method 1 and Method 3. As shown in Figure 7e,f, due to the improvement in the command value of DC current, the trigger angle under Method 2 was smaller than that under Method 1 and Method 3. The reduced amount of variation in the active power fed to the rectifier station under Method 2 is shown in Figure 7h. The reduced active power and reactive power imbalance prevented the AC transient overvoltage. As shown in Figure 7g, the improved control had a limited impact on the inverter station. No subsequent commutation failure occurred under the three methods.

5.2. Under Different Short-Circuit Ratios

The short-circuit ratio of the sending-end grid was changed to 1.5 and 3, respectively. The three-phase fault occurred at 1 s. The fault duration was 0.1 s. The electrical quantities of LCC-HVDC under different short-circuit ratios are shown in Figures 8 and 9, respectively.

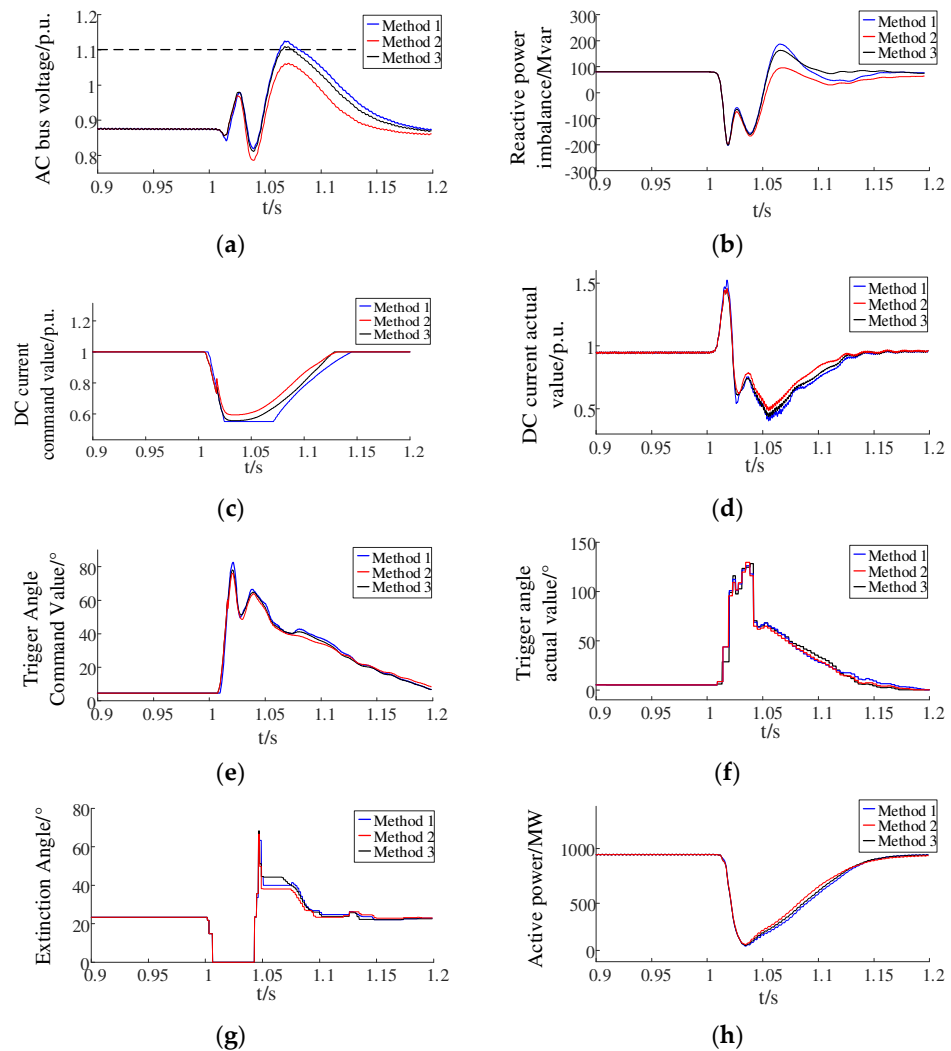


**Figure 8.** Electrical quantities of LCC-HVDC (SCR = 1.5). (a) AC bus voltage at the rectifier station; (b) Reactive power imbalance; (c) Command value of DC current at the rectifier station; (d) DC current actual value of the rectifier station; (e) Trigger angle command value of the rectifier station; (f) Trigger angle actual value of the rectifier station; (g) Extinction angle of the inverter station; (h) Active power fed to the rectifier station.

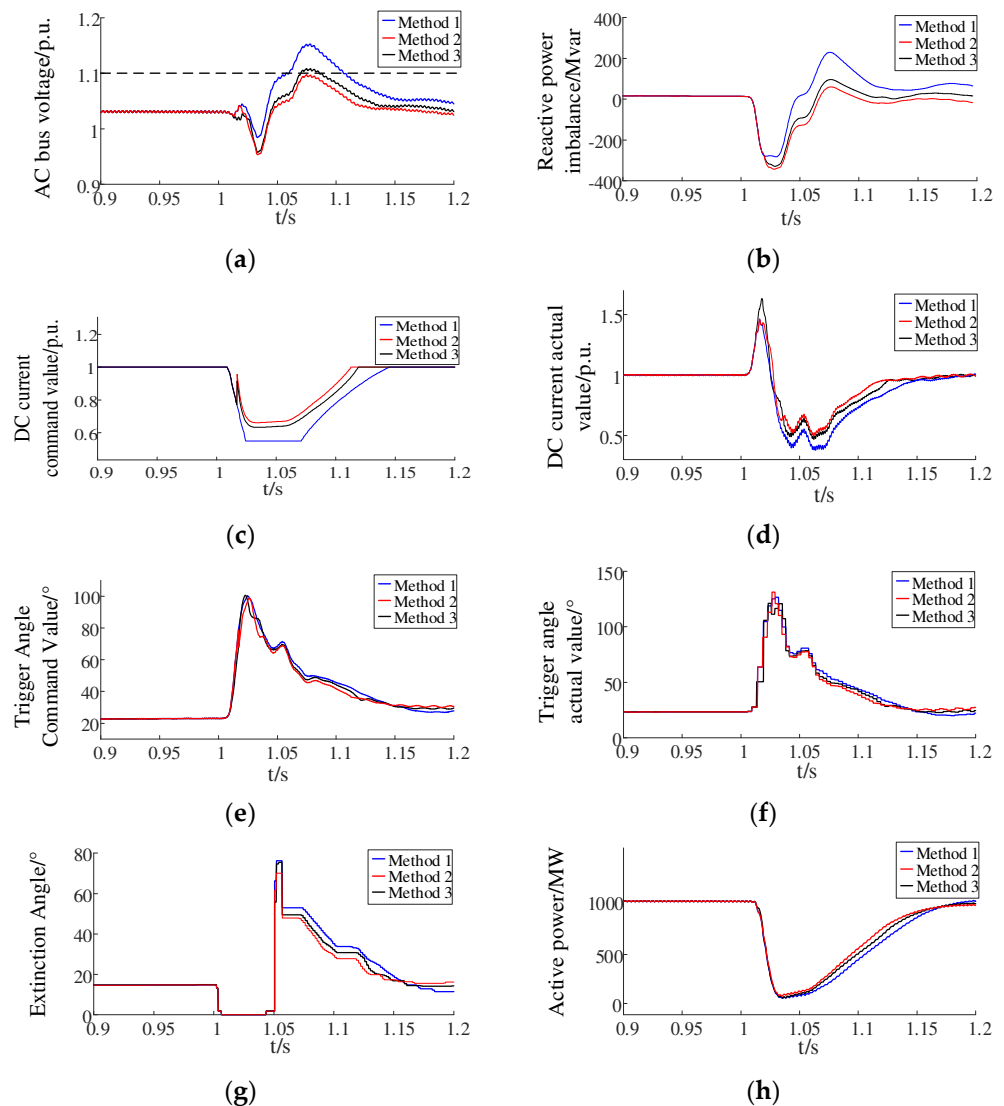


**Figure 9.** Electrical quantities of LCC-HVDC (SCR = 3). (a) AC bus voltage at the rectifier station; (b) Reactive power imbalance; (c) Command value of DC current at the rectifier station; (d) DC current actual value of the rectifier station; (e) Trigger angle command value of the rectifier station; (f) Trigger angle actual value of the rectifier station; (g) Extinction angle of the inverter station; (h) Active power fed to the rectifier station.

The commutation failure occurred after a three-phase fault. When the short-circuit ratio was 1.5, the maximum AC bus voltage under Method 2 was 1.066 p.u., while the maximum AC bus voltages under Method 1 and Method 3 were, respectively, 1.114 p.u. and 1.130 p.u., as shown in Figure 8a. The AC bus voltage was suppressed to below the allowable voltage threshold under Method 2. Compared with the case with the short-circuit ratio of 2.5, the smaller the short-circuit ratio was, the greater the effect of the AC-DC system coupling was, and the greater the AC bus voltage under Method 3 was.

As shown in Figure 8b–d, the DC current under Method 2 was greater than that under Method 1 and Method 3. Therefore, the reactive power imbalance under Method 2 was smaller. The trigger angle under Method 2 was smaller than that under Method 1 and Method 3, as shown in Figure 8e,f. The variation in the active power fed to the rectifier station under Method 2 was also smaller, which caused the AC bus voltage to decrease, as shown in Figure 8h. As shown by Figure 8g, none of the three methods caused a subsequent commutation failure. The AC transient overvoltage was effectively prevented by Method 2, on the condition of normal commutation.

When the short-circuit ratio was 3, as shown in Figure 9a, the maximum AC bus voltages under Method 1 and Method 3 were 1.152 p.u. and 1.108 p.u., respectively. Compared to Method 1 and Method 3, the AC bus voltage under Method 2 was smaller, with a maximum value of 1.094 p.u. The AC transient overvoltage was effectively limited to below the allowable voltage threshold under Method 2. The suppression of the AC transient overvoltage by Method 3 under a short-circuit ratio of 3 was better than that under a short-circuit ratio of 1.5. However, the AC bus voltage under Method 3 still exceeded 1.1 p.u.

The DC current under Method 2 was greater than that of Method 1 and Method 3, which reduced the reactive power imbalance, as shown in Figure 9b–d. As shown in Figure 9e,f, the command and actual values of the trigger angle under Method 2 were smaller than those of Method 1 and Method 3. Meanwhile, the variation in the active power fed to the rectifier station under Method 2 was also smaller than that of Method 1 and Method 3, as shown in Figure 9h. There were no subsequent commutation failures under the three methods. The effectiveness of Method 2 was fully verified.

## 6. Conclusions

The inverter station of LCC-HVDC is susceptible to commutation failures, resulting in an increase in the AC bus voltage at the rectifier station, and AC transient overvoltage in the sending-end grid. Due to the interdependence of the DC current with the active power and reactive power consumption of the rectifier station, changes in active and reactive power produce variations in the AC bus voltage of the rectifier station. Therefore, AC transient overvoltage cannot be prevented by adjusting reactive power only. Thus, the coupling effects among power, AC bus voltage, and DC current on AC transient overvoltage were explored. A dynamic model of the AC bus voltage of the rectifier station was built to depict the AC-DC system coupling. Furthermore, a calculating method for the command value of the DC current was proposed based on the model of predictive control. Therefore, an improved suppression method for AC transient overvoltage was formed with consideration. The AC transient overvoltage was effectively suppressed through adaptively regulating the DC current at the rectifier station, because the influencing factors of AC transient overvoltage were comprehensively taken into account.

**Author Contributions:** Conceptualization, J.O., Y.C., X.P. and Y.D.; methodology, J.O., Y.C. and X.P.; software, X.P. and Y.D.; validation, X.P.; formal analysis, J.O. and Y.C.; investigation, Y.C. and X.P.; resources, J.O. and Y.C.; data curation, Y.C. and X.P.; writing—original draft preparation, Y.C. and X.P.; writing—review and editing, J.O., Y.C., X.P. and Y.D.; visualization, X.P. and Y.D.; supervision, J.O. All authors have read and agreed to the published version of the manuscript.

**Funding:** This research received no external funding.

**Data Availability Statement:** The data used to support the findings of this study are available from the corresponding author upon request.

**Conflicts of Interest:** The authors declare no conflicts of interest.

## References

1. Muniappan, M. A comprehensive review of DC fault protection methods in HVDC transmission systems. *Prot. Control Mod. Power Syst.* **2021**, *6*, 1–20. [[CrossRef](#)]
2. Ouyang, J.; Zhang, Z.; Li, M.; Pang, M.; Xiong, X.; Diao, Y. A predictive method of LCC-HVDC continuous commutation failure based on threshold commutation voltage under grid fault. *IEEE Trans. Power Syst.* **2020**, *36*, 118–126. [[CrossRef](#)]
3. Xue, Y.; Zhang, X.; Yang, C. Elimination of Commutation Failures of LCC HVDC System with Controllable Capacitors. *IEEE Trans. Power Syst.* **2016**, *31*, 3289–3299. [[CrossRef](#)]
4. Xue, Y.; Zhang, X.; Yang, C. Commutation failure elimination of LCC HVDC systems using thyristor-based controllable capacitors. *IEEE Trans. Power Deliv.* **2018**, *33*, 1448–1458. [[CrossRef](#)]
5. Tu, J.; Zhang, J.; Zeng, B.; Liu, M.; Yi, J.; Bu, G. HVDC Transient Reactive Power Characteristics and Impact of Control System Parameters during Commutation Failure and Recovery. *High Volt. Eng.* **2017**, *43*, 2131–2139.
6. Yin, C.; Li, F. Analytical expression on transient overvoltage peak value of converter bus caused by DC faults. *IEEE Trans. Power Syst.* **2021**, *36*, 2741–2744. [[CrossRef](#)]

7. Nian, Y.; Jin, X.; Li, G. Influence of UHV DC Commutation Failure on the Transient Reactive Power Characteristics of Wind Turbines in Sending Terminal Grid. *Proc. CSEE* **2020**, *40*, 4111–4122.
8. Zhao, X.; Li, Y.; Sun, G.; Zhang, Y.; Zeng, L. Effect of Commutation Failure on the Overvoltage on Rectifier Station in AC/DC Hybrid Power System with Wind Farms. *High Volt. Eng.* **2019**, *45*, 3666–3673.
9. Yue, H.; Shao, G.; Xia, D.; Sun, M.; Liu, Y.; Wang, K. Reactive Power Control Strategy for UHVDC Weak Sending-end System Considering Overvoltage Suppression. *Autom. Electr. Power Syst.* **2020**, *44*, 172–179.
10. Sun, W.; Cui, C.; Zhou, X.; Li, X.; Fu, Y.; Li, C.; Lei, Y.; Dai, G.; Kang, J. Coordinated control strategy for synchronous condenser and AC filter in UHVDC converter station. *Power Syst. Prot. Control* **2020**, *48*, 182–187.
11. Zhu, L.; Liu, W.; Shao, C.; Xu, H.; Niu, S. Control strategy of suppressing wind turbine tripping based on coordination between synchronous condenser and SVC in sending-end network of HVDC. *Electr. Power Autom. Equip.* **2021**, *41*, 107–115.
12. Li, W.; Qian, Z.; Wang, Q.; Wang, Y.; Liu, F.; Zhu, L.; Cheng, S. Transient voltage control of sending-end wind farm using a synchronous condenser under commutation failure of HVDC transmission system. *IEEE Access* **2021**, *9*, 54900–54911. [[CrossRef](#)]
13. Ji, X. Optimization of HVDC Control System for Mitigating AC Transient Overvoltage on Rectifier Station. *Power Syst. Technol.* **2017**, *41*, 721–728.
14. Wang, T.; Pei, L.; Wang, J.; Wang, Z. Overvoltage Suppression Under Commutation Failure Based on Improved Voltage-Dependent Current Order Limiter Control Strategy. *IEEE Trans. Ind. Appl.* **2022**, *58*, 4914–4922. [[CrossRef](#)]
15. Yin, C.; Li, F. Reactive Power Control Strategy for Inhibiting Transient Overvoltage Caused by Commutation Failure. *IEEE Trans. Power Syst.* **2021**, *36*, 4764–4777. [[CrossRef](#)]
16. Qin, Y.; Yin, C.; Duan, Q.; Ma, X. Research on transient voltage characteristics and support strategy under a fault occurred in the near-zone of HVDC sending system. *Power Syst. Prot. Control* **2023**, *51*, 169–177.
17. Zhao, D.; Guo, C.; Ye, Q.; Fan, X.; Zhao, Z.; Li, T. Reactive power decentralized cooperative control method for restraining AC transient overvoltage of wind farm via LCC-HVDC grid-connected system. *Electr. Power Autom. Equip.* **2024**, *44*, 88–94.
18. Liu, C.; Zhang, B.; Sun, H. Sensitivity Analysis for AC/DC Hybrid Power Systems. *Power Syst. Technol.* **2006**, *30*, 35–41. [[CrossRef](#)]
19. Xu, Z. AC/DC and DC/DC Interactions of Multiple HVDC Links Terminating in the Same AC System. *Power Syst. Technol.* **1998**, *22*, 18–21. [[CrossRef](#)]
20. Wu, P.; Xu, S.; Zhao, B.; Chen, H. Research of weak sending-end coupling characteristics for bundled wind-thermal power transmission of UHVDC project. *Electr. Power Autom. Equip.* **2016**, *36*, 60–66.
21. Aik, D.L.H.; Andersson, G. Use of participation factors in modal voltage stability analysis of multi-infeed HVDC systems. *IEEE Trans. Power Deliv.* **1998**, *13*, 203–211. [[CrossRef](#)]
22. Han, L.; Yin, C.; Dai, C.; Ma, X. Transient voltage operational risk of a high-proportion new energy sending system. *Power Syst. Prot. Control* **2024**, *52*, 23–34.
23. Lin, S.; Lan, F.; Liu, J.; Li, X. Overview of transient overvoltage mechanism and suppression strategies of high voltage direct current transmission grid. *J. Electr. Power Sci. Technol.* **2022**, *37*, 3–16.
24. Ouyang, J.; Pan, X.; Ye, J.; Xiao, C.; Diao, Y.; Zhang, Q. An improved prediction method of subsequent commutation failure of an LCC-HVDC considering sequential control response. *Prot. Control Mod. Power Syst.* **2023**, *8*, 46. [[CrossRef](#)]
25. Ouyang, J.; Ye, J.; Zhang, Z.; Diao, Y. Prevention control method of subsequent commutation failure for LCC- HVDC under grid fault. *Int. Trans. Electr. Energy Syst.* **2021**, *31*, 12–25. [[CrossRef](#)]
26. Fei, L.; Wang, T.; Zhao, W.; Wang, C.; Wang, J.; Sun, Y. Analysis of the influence of virtual inertial control on the transient overvoltage of the wind-thermal-bundled sending system in the scenario of commutation failure. *Power Syst. Technol.* **2024**, 1–11. [[CrossRef](#)]
27. Han, P.; Zhang, H.; Ding, M.; Zhang, Y.; Chen, L.; Li, B. A Coordinated HVRT Strategy of Large-Scale Wind Power Transmitted with HVDC System. *Power Syst. Technol.* **2018**, *42*, 1086–1095.
28. Szechtman, M.; Wess, T.; Thio, C.V. A Benchmark Model for HVDC System Studies. In Proceedings of the AC and DC Power Transmission International Conference, London, UK, 17–20 September 1991; pp. 374–378.

**Disclaimer/Publisher’s Note:** The statements, opinions and data contained in all publications are solely those of the individual author(s) and contributor(s) and not of MDPI and/or the editor(s). MDPI and/or the editor(s) disclaim responsibility for any injury to people or property resulting from any ideas, methods, instructions or products referred to in the content.